HANDBOOK OF MEASUREMENT IN SCIENCE AND ENGINEERING

Volume 2

Edited by

MYER KUTZ

Handbook of Measurement in Science and Engineering is available online in full color at http://onlinelibrary.wiley.com/book/10.1002/9781118436707.

WILEY

A JOHN WILEY & SONS, INC., PUBLICATION

36

OPTICAL METHODS FOR THE MEASUREMENT OF THERMAL CONDUCTIVITY

PRABHAKAR R. BANDARU AND MAX S. AUBAIN

36.1 THERMAL BOUNDARY RESISTANCE MAY LIMIT ACCURACY IN CONTACT-BASED THERMAL CONDUCTIVITY (κ) MEASUREMENTS

The issue of heat transport in materials has a long and venerable history ranging from the early investigations of Fourier. The efforts have been mostly focused on the

Handbook of Measurement in Science and Engineering, 2V Set, First Edition. Edited by Myer Kutz.

estimation of the thermal conductivity (κ) based on the widely accepted relationships below, which relate the heat flux (Q) to the temperature difference (ΔT), with the thermal conductance (K) as the constant of proportionality, and the heat flux through an equivalent cross-sectional area (A) to the temperature gradient ($\nabla \cdot T$) across a specified length (L).

$$Q = K\Delta T \tag{36.1a}$$

$$Q = -\kappa A \nabla \cdot T \tag{36.1b}$$

From geometrical considerations ($K = \kappa[A/L]$). The conventional method of the κ determination then use steady-state or transient/time-dependent measurements, incorporating the analysis of the heat conduction equation at any position, r, and time, t, i.e.,

$$\frac{\partial T(r,t)}{\partial t} = \nabla \cdot [\kappa(r,t) \cdot \nabla \cdot T(r,t)] \tag{36.2}$$

Equation (36.2) is solved with respect to specified boundary conditions (Carslaw and Jaeger, 1986; Ozisik, 1968), and the isotropic value of the κ ($\equiv \kappa(r,t)$) are the values that are widely reported.

However, a major issue in such methods is the use of physical contacts, which serve for heat transfer from the heater (which generates the Q) into the material that needs to be characterized. Now, it is well known that the thermal boundary resistance (R_{TBR}) (Swartz and Pohl, 1989) due to contact-material interfaces could limit the thermal conductivity/conductance (Chen, 1998). An additional thermal resistance (= $1/K$)/unit area, R_{TBR} would then contribute to obtain an apparent value of the thermal conductivity (i.e., κ_{app}), which is really the value being measured/reported and not the true/intrinsic value (i.e., $\kappa_{int} \equiv \kappa$), that is, through

$$R_{app}\left(=\frac{L}{\kappa_{app}}\right) = R_{TBR} + R_{int}\left(=\frac{L}{\kappa_{int}}\right)$$

From a physical point of view, the heat transport across the interface of the contact and the material could be significantly affected by the thermal boundary resistance (TBR), which mainly arises due to the reflection, transmission, or absorption of heat-carrying phonons (collective lattice vibrations) (Kittel, 1996) at the interface. In addition, the surface/interface beneath the thermal energy sensors (e.g., thermocouples and thermometers) would also modulate heat flow and lead to errors/spurious readings, and so on. Consequently, much effort has been expended to provide an explanation and to account quantitatively for the influences of the TBR on thermal conductivity measurements. At the very outset, since interface conditions are mostly unpredictable (unless extreme care is taken to test with materials under specialized conditions, vacuum, cryogenic temperatures, etc. the used phenomenological models are at best approximate and serve only as a guide or provide limits for the effects of the TBR.

Such models were first quantitatively discussed in detail for solid–liquid Helium interfaces, which were posited to have an associated Kapitza resistance (Pollack, 1969).

The corresponding Kapitza resistance/TBR between materials was then found to depend on the ratio of the materials' Debye temperatures (Stoner and Maris, 1993). It was proposed that a ratio close to one could result in a closer match of the phonon wavelengths and enhanced phonon transmission, compared to when the ratio was much different than unity, cf., 0.05 for a lead–diamond interface. In this context, two basic models, that is, (1) the acoustic mismatch model (AMM) and (2) the diffuse mismatch model (DMM) have been used (Swartz and Pohl, 1989) to understand the κ in the context of conduction across an interface/boundary. In the AMM, the constituents on either side of the interface are treated as bulk solids, in a continuum approximation, with an associated acoustic impedance, Z ($= \rho v$), where ρ is the bulk material density and v the associated acoustic velocity. The heat flux across the interface is then determined (Little, 1959) by the product of the incident number of phonons and the transmission probability, which in turn is inversely proportional to the relative contrast in the Z values of the materials constituting the interfaces, for example, the maximum transfer of heat occurs when the two materials have identical Z values. Due to the materials being modeled as continua, the detailed nature of the interface is ignored in the AMM approximation, that is, the phonon wavelength (λ_{ph}) > interface roughness. However, at increasing phonon energy/decreasing λ_{ph}, the phonon mean free path (l) could be comparable to the scale of surface roughness and imperfections, and the AMM would be inappropriate (Swartz and Pohl, 1989; Little, 1959).

Alternately, the diffuse mismatch model (DMM) implicitly considers the detailed nature of the interface through considering individual phonon traversal. The phonons impinging on the interface lose memory of their original state (direction, polarization, etc.) subsequent to scattering. The transmission of any phonon is now determined by whether there is a corresponding phonon, on the other side, of same energy to which scattering can occur, that is, by the phonon distribution or the density of states (DOS), $g(\omega)$. Although both the AMM and the DMM have been applied to simulate experimental situations, their simplified formulation considering primarily elastic scattering, generally precludes universal agreement (Swartz and Pohl, 1989) with practical situations. For example, in the case of SiO_2 and SiN_x films deposited on Si substrates, the DMM was shown to yield good agreement at low temperatures (<20 K) while it differed from experimental observations by an order of magnitude at room temperature (Lee and Cahill, 1997). Typically the DMM, which considers a greater number of phonons elastically scattering would be thought to predict a higher thermal conductance/conductivity compared to the AMM (Lee and Cahill, 1997). Indeed, the highest K, corresponding to the phonon radiation limit, is manifested through the DMM (Swartz and Pohl, 1989). However, inelastic scattering processes, for example, due to point defects (Koh et al., 2009), interfacial roughness, tunneling, excitation of surface phonons, phonon down-conversion (Kelly, 1985), and influence of electrical carriers, or strain at the interface are not considered in either model and make detailed prediction difficult.

To understand the interface scattering in more detail, molecular dynamics (MD) simulations, which serve to check the diffusive approximations inherent in the Boltzmann transport formalism underlying the Fourier relationships have been attempted (Chen et al., 2004). In MD, mutual atom–atom interactions, for example, modeled through Lennard–Jones (Kittel, 1996; Chen et al., 2004) or other inter-atomic potentials (Volz and Chen, 1999) are considered, and the heat flux computed from the product of the atomic forces and velocities.

36.2 OPTICAL MEASUREMENTS OF κ MAY AVOID CONTACT-RELATED ISSUES

Considering the unpredictable influences of the contacts, it was recognized that noncontact methodologies for measurement of κ, for example, using optical beams to provide both heating and subsequently probe temperature gradients/distributions, could provide an alternative. In this regard, a "flash method" was proposed in 1961 (Parker et al., 1961) whereby a discharge from a flash lamp (of 400 J in energy) was incident on the front surface of a sample (1–3 mm in thickness) and analysis of the time (t) variation of temperature (T) at the back surface of the sample correlated to the thermal diffusivity ($\alpha = \kappa/C\rho$), where C is the specific heat and ρ the material density—Figure 36.1. It was noted that the C can be determined through the maximum temperature rise at the back surface. Generally, such transient-based techniques have an advantage over steady-state methods in that the T–t curves can be generated, which implicitly contain the diffusivity parameter, and a single experiment can be used to deduce the values of κ, C, and α. The flash method, now using laser pulses, has since been subject to extensive development, for example, by NETZSCH® Instruments (N. T. Analysis, http://www.netzsch-thermal-analysis.com/), in the commercial sector. It is then indeed remarkable that the determination of α could be reduced to $\left(= 0.1388 \times l^2/t_{1/2}\right)$ where the l is the sample thickness and $t_{1/2}$ the "time at 50% of the temperature increase measured at the rear of the test sample in seconds"—taken from the laser flash apparatus (LFA) 427 brochure at NETZSCH.

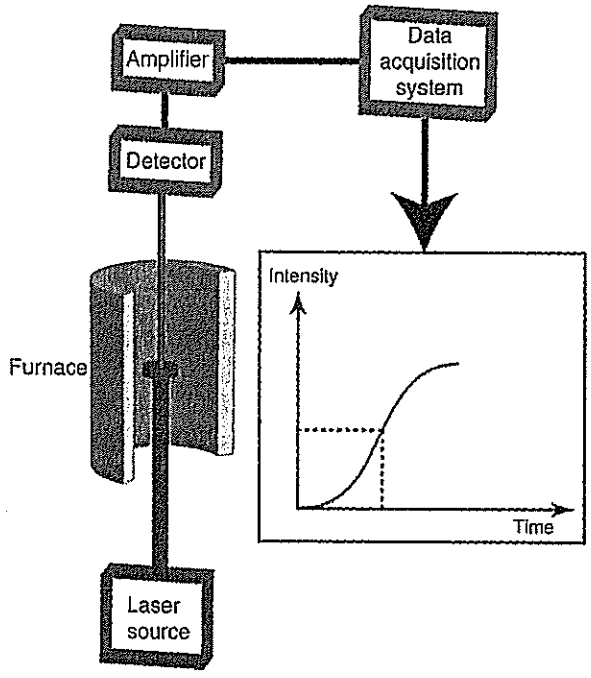

FIGURE 36.1 Schematic of laser flash apparatus (LFA) used to measure the thermal conductivity (adapted from the LFA 427 brochure at NETZSCH).

However, issues with nonuniform heating over a finite heating spot area, the accuracy of the temperature monitoring system, and the proper fitting of the T–t curves (considering possible heat losses) all have to be considered (Baba and Ono, 2001) and calibrated to yield a precise value of the thermal diffusivity. Correspondingly, monitoring the heat pulse propagation (originating, say, from an electrical current pulse) at locations on the sample away from the contacts could also be used to determine κ and C through computation of the statistical moments of the T–t curve ($\int_0^\infty \Delta T(x,t)t^n\,dt$ for $-\infty < n < \infty$) (Arriagada et al., 2009).

36.2.1 Probing κ in Lower Dimensional Structures (Thin Films and Nanostructures)

While measurements on bulk materials (defined by a thickness adequate to permit the diffusion of the heat from the pulse and establish a T–t profile where the temperature at the surface, T_s decays to at least a value of $(1/e)\,T_s$, (where e is the base of the natural logarithm) at the back surface of the sample) are enabled adequately through the laser flash-based methods, new challenges arise in the measurement of thin films. An estimate of the thickness at which the flash methods, as described previously, may not be adequate can be deduced through the diffusion length $L \sim \sqrt{\alpha t}$ [The $(1/e)\,T_s$ and the $L \sim \sqrt{\alpha t}$ are rules of thumb given that a common time-dependent solution for $T(r,t)$ from Equation (36.2) varies as exp $(-cL^2/\alpha t)$, where c is a numerical constant). As an average value of α for solids is of the order of 1 cm^2/s and that the time resolution can be 0.1 ns (with state-of-the-art, fast sampling oscilloscopes at 10 GS/s), the minimum thickness is of the order of 100 nm. As thin films of around this thickness are used extensively, for example, in the semiconductor industry (Ohring, 2002; Sze and Ng, 2006), and as the thin films are deposited on substrates, an alternate technique is required to measure the intrinsic κ of the film, free of the influence of the substrate.

Higher time resolution measurements would then be required and are provided through transient thermoreflectance (TR)-based techniques (Paddock and Eesley, 1986). A "pump-probe" methodology is invoked, where initially a pump mode-locked Ti-sapphire laser (Saleh and Teich, 2007) with pulse width <1 ps and pulse intensity 1–10 nJ/pulse corresponding to mW powers (Capinski et al., 1999; Schmidt et al., 2008) is incident onto and heats the thin film sample. The heating modifies the refractive index, and hence changes the reflectivity of the film which to a first approximation is proportional to the temperature change, ΔT (also see Section 36.2.2). The reflectivity is subsequently probed, after a calibrated time delay, through a weaker intensity (of the order of 0.01 nJ/pulse) probe laser. The probe laser beam can either be distinct or can be referenced to the pump laser (through an attenuator) and needs to be focused onto the heated spot, quite accurately (Capinski and Maris, 1996). The spatial resolution of the incident laser spot is diffraction limited and is typically 5–10 μm and the laser beam penetration is of the order of the electromagnetic skin depth (Fox, 2001), which is ~20 nm (at a laser wavelength ~633 nm and material resistivity of ~0.1 Ω cm). Such a large aspect ratio, between the spot size and the skin depth, essentially ensures one-dimensional heat flow from the surface downward and could be thought to measure cross-plane thermal conductivity. The reader can consult additional references on the discussion of optical methods such as Raman spectroscopy (Christofferson et al., 2008) and charge-coupled device (CCD)-based image acquisition methods (Christofferson et al., 2008), which have also been used to map temperature distributions.

36.2.2 Probing the Anisotropy in the κ

Generally, while material thermal conductivity (κ) is traditionally defined from the ratio of the heat flux to the temperature gradient as a second-rank tensor, it is typically regarded as a scalar and an isotropic materials property. Anisotropy in the thermal conductivity is not generally considered even in thin films or even in one-dimensional nanostructures, such as nanowires (Boukai et al., 2008) or nanotubes (Bandaru, 2007) where anisotropy could be thought to be obviously present, for example, intuitively the κ values along and perpendicular to a strictly two-dimensional film or a one-dimensional wire would not be expected to be the same (a structure is effectively n-dimensional if the length in the $(3-n)^{\text{th}}$ dimension/s is less than the λ_{ph}—in the case of thermal conductivity). Limits to κ should then be considered, for example, in terms of the mean free path, l and particular phonon wavelength, λ_{ph}, especially when the relevant length scales in the film approach the carrier mean free path (Chen, 1998; Sondheimer, 1952; Baillis and Randrianalisoa, 2009; Narumanchi et al., 2004).

Although substantial progress has been made in the past few years in understanding heat conduction in lower dimensional structures (Cahill et al., 2003; Chen and Shakouri, 2002) many issues are still unresolved. There is still difficulty in accurate measurement (Cahill et al., 2002), and precise understanding of the phonon interactions with interfaces/boundaries has not yet been obtained. In case of thin films, a few attempts have been made to correlate possible anisotropies to film and measurement geometry (Borca-Tasciuc et al., 2001), where for example, a variation dependent on the direction heat flow, cross-plane (κ_{cp}) or in-plane (κ_{ip}), was noted. The discussion has then largely been framed on the basis of the classical (Kittel, 1996) interpretation of the κ, as the product of the specific heat capacity (C), the phonon group velocity (v), and the mean free path (l) that is, $\kappa \sim Cvl$. Although the assumptions of classical mechanics are inadequate to explain electron motion, due to the spin degree of freedom, classical modeling is typically considered adequate for phonons.

It then naturally follows that a reduction of any of the constituent terms would reduce the κ. As such, a reduction cannot be surmised from an elementary formulation of the Fourier heat conduction problem, and various phonon transport models have then been considered (Narumanchi et al., 2005)—ranging from the "gray" approximation where all the phonons (both acoustic and optical) are taken as equally contributing to the heat transport to "semi-gray" models (Chen and Shakouri, 2002; Chen, 2000) where mostly longitudinal acoustic (LA) phonons contribute while optical phonons are relatively stationary due to their small dispersion and group velocity. A relative partitioning of the C values between the acoustic and optical phonons also results. A further improvement on the previous considerations arises through consideration of the phonon dispersion in the first Brillouin Zone (BZ), typically considered isotropic (Dolling and Cowley, 1966), through polynomial fits to the experimental spectra (Baillis and Randrianalisoa, 2009). The resulting $\omega - k$ fits can then be utilized to determine the frequency dependent v, while the C can be estimated through taking the temperature derivative of the total energy obtained by integrating the fits over the BZ (Kittel, 1996). However, the remaining factor in the thermal conductivity expression, l is not amenable to analytical calculation/fitting as it depends on the influencing (Peierls, 1955) intimate details of the underlying material, such as anharmonic interactions, defects and impurities, and surface corrugation, which are rarely the same in any two particular material structures. The sensitivity of the l to such details is quite difficult to determine theoretically and, due to its importance for

the κ, needs to be experimentally probed. For example, when one considers the l as a vector, with decomposition into three orthogonal components in a rectangular coordinate system, l_x, l_y, and l_z, there would be three corresponding values of the κ, κ_x, κ_y, and κ_z. Limits to l could be also considered, for example, in terms of the mean free path and particular phonon wavelength, especially when the relevant length scales approach the carrier mean free path (Chen, 1998; Sondheimer, 1952; Baillis and Randrianalisoa, 2009; Narumanchi et al., 2004). Presently, there are very few reports on the experimental determination of the thermal conductivity tensor (Quelin et al., 1993), and typically the isotropic value is suggested (Che et al., 2000). It is then of interest to explore experimental methods for the determination of the κ tensor, which could then yield insight into the relevance of the isotropy assumption. It could be reasonably expected that the effects of anisotropy would be increasingly manifest in lower symmetry crystal structures as well as lower dimensional materials, such as two-dimensional thin films or one-dimensionally oriented nanowires.

We then consider exploring anisotropy in the thermal conduction through exploring a prototypical system incorporating thin films of silicon arranged on an insulating substrate. In addition to its immense technological usage, silicon can be configured in silicon-on-insulator (SOI) structures, where Si thin films can be prepared with varying thickness (from an atomic layer upward) on an underlying oxide of low thermal conductivity ($\sim$1.4 W/mK). The advantage of the SOI manifold is that the Si thin films can be considered to be approximately thermally independent of the underlying structure. Such a configuration permits the characterization of thin films, say $<$100 nm in thickness, that would be too difficult to handle in practice. However, it should be noted that while the Si films are typically close to single-crystalline, processing could introduce random defects/impurities. In addition to enabling easier experimentation (the alternate would be to suspend the Si through complicated etching procedures), the SOI structure is commercially used in electronic devices, where it has been indicated that up to a 25% increase in speed concomitant with a 50% reduction in the consumed power is achievable (Sze, 2003). However, enhanced electronic switching performance is coupled with enhanced heat production (Pop, 2010), the dissipation of which is a major issue with SOI-based structures.

It is then of much scientific and technological interest to investigate thermal conduction issues through Si thin films in SOI structures. This involves first, the determination of both the κ_{cp} and κ_{ip} (assuming that the in-plane conduction is isotropic). At present, the majority of the experiments involve periodic surface heating—at an angular frequency—ω, though an electrical resistor, for example, as in the 3ω method (Cahill, 1990) where a metal line serves as both the heater and the thermometer, or through the use of a pump laser, for example, as in time domain thermoreflectance (TDTR) (Paddock and Eesley, 1986; Capinski et al., 1999) or frequency domain thermoreflectance (FDTR) (Schmidt et al., 2009). The thermal conductivity is deduced through an analysis of the measured signal, for example, the third harmonic of the voltage in the 3ω method or through the change in reflectance of the surface from a probe laser in TDTR, the physical basis of which is the spread of the thermal wave in the underlying films/layers. Although heat from a point source would diffuse radially, the use of metal lines of finite width or pump laser spot diameters of much greater than the thermal penetration depth (TPD) $\sim \sqrt{\kappa/\omega C}$, results in quasi-one-dimensional heat transfer and the probing of the κ_{cp}. A few corrections in the measurement of the κ_{cp}, to account for the degree of orthogonal heat flow have been described (Borca-Tasciuc et al., 2001) to understand the relative influences of the TPD, heater width, underlying layer thickness, and thermal conductivity

anisotropy, and other geometry dependent correction factors in the 3ω method. Alternately, in TDTR/FDTR methods, the effects of heat accumulation (e.g., when the material does not reach its unperturbed state between two successive laser heating pulses) on radial heat transfer have been probed (Schmidt et al., 2008) and used to extract the in-plane and cross-plane thermal conductivity values of highly oriented pyrolytic graphite (HOPG). Generally, a greater sensitivity to lateral heat spreading would be achieved with an underlayer of low κ due to the slower diffusion of heat from the heating spot.

Although the above state-of-the-art methodologies may yield some measure of the anisotropy of the thermal conductivity, they nevertheless provide an indirect measure. It would be desirable to develop a simpler method for measuring the anisotropy in any material. One possible methodology, in the spirit of the above discussion, involves correlating the changes in the optical reflectance to the temperature (Rosencwaig et al., 1985), which would be most suitable for a noncontact method and which mitigates issues such as boundary resistances and heater capacitances (Borca-Tasciuc et al., 2001). The concomitant difficulties are the sensitivity of the measured signal-to-surface conditions and wavelength (Tessier et al., 2003). As mentioned earlier, the SOI structure would be an ideal platform to consider thermal conductivity anisotropy through TR measurements, the principles of which will now be discussed in detail.

36.3 THERMOREFLECTANCE (TR)

36.3.1 Principles

TR involves experimental methods which allow for noninteractive interrogation of the relative or absolute temperature of a surface or interface of a metallic or semiconducting material, enabled through the temperature dependence of the material's electronic energy levels and macroscopically manifested through the dielectric constant (ε) and change in the measured reflectance.

A little more specifically, the response incorporates the effects of temperature increase/heating through a shift of the electron/hole Fermi energy in metals or semiconductors, which in turn modulates the light absorption characteristics and reflectivity (Fox, 2001). Hence, the heating of an electrically conducting material can be measured optically and the extent of heating would be a function of the inherent thermal conductivity. The thermal modulation of reflected light from semiconductors was initially used to study band structure (Berglund, 1966), and such a method was concomitantly exploited for the study of heat transport. One advantage was that it allowed for temperature mapping of arbitrary sample surface geometries. This feature has great utility in understanding thermal transport in microelectronics and MEMS where "hot spots" can easily develop. In addition, as this optical method is noninteracting, it may allow for the thermal measurement of sensitive nanoscale devices such as nanowires or suspended structures.

The TR signal, with respect to the total reflected amplitude, is typically two to five orders of magnitude smaller and requires highly sensitive detection techniques. The response is also dependent on the wavelength of light used (Tessier et al., 2001, 2003), surface condition, and the existence of transparent overlayers (Ju and Goodson, 1998; Maize et al., 2008; Tessier et al., 2006). Using modified microscopes or other custom-built CCD-based setups, temperature resolutions of 10 mK and diffraction-limited spatial resolutions are fundamentally possible and have nearly been achieved (Mayer et al., 2006).

TR relies on the dependence of the reflectivity of a material, which for example, can be described through the change in refractive index or, equivalently, the change in dielectric constant due to temperature. The reflectivity of the surface of a material with respect to a normal, incident electromagnetic wave is defined as

$$R = \left(\frac{\tilde{n}-1}{\tilde{n}+1}\right)^2 \tag{36.3}$$

where $\tilde{n}$ is the wavelength-dependent complex refractive index, $\tilde{n} = n + ik$, with the real part, n proportional to the bending of the light, while k represents the light attenuation. Differentiating and normalizing the R gives the contribution due to the change in both Δn and attenuation constant, Δk:

$$\frac{\Delta R}{R} = \frac{4(n^2 - k^2 - 1)\Delta n + 8nk\Delta k}{\left[(n+1)^2 + k^2\right]\left[(n-1)^2 + k^2\right]} \tag{36.4}$$

The above can be expressed equivalently through the variation of the complex dielectric constant, $\tilde{\varepsilon}(= \tilde{n}^2) = \varepsilon_1 + i\varepsilon_2$, as:

$$\frac{\Delta R}{R} = \frac{2A}{A^2 + B^2}\Delta\varepsilon_1 + \frac{2B}{A^2 + B^2}\Delta\varepsilon_2 \tag{36.5}$$

where $A = n\,(n^2 - 3k^2 - 1)$ and $B = k\,(3n^2 - k^2 - 1)$.

In a semiconductor, a temperature change could be considered to be manifested through the modulation/change of the fundamental energy band gap, E_g, whereby $\Delta\tilde{\varepsilon} = (\partial\tilde{\varepsilon}/\partial E_g)\,(\partial E_g/\partial T)\,\Delta T$. Such a relation considers that the material characteristics (e.g., thermal expansion and density) are relatively unchanged implying a low ΔT and from the above, the relative change in reflectance, $\Delta R/R$, is linearly proportional to the temperature, that is,

$$\frac{\Delta R}{R} = \frac{1}{R}\frac{\mathrm{d}R}{\mathrm{d}T}\Delta T = C_{\mathrm{TR}}\Delta T$$

where C_{TR} is defined as the TR coefficient. The C_{TR} then incorporates various materials parameters and is quite sensitive, for example, to the surface (which changes the R) making published values (typically in the range 10^{-4} to 10^{-5} K^{-1} for metals and 10^{-3} for semiconductors) more useful as a guideline, rather than a reference. Consequently, the determination of C_{TR} needs calibration for an individual sample surface.

36.3.2 Thermoreflectance to Measure the κ of Thin Films

We now illustrate, through a specific case study, the practical usage of TR to measure thermal conductivity of thin films. Such a study is also aimed at a preliminary understanding of the issues of κ anisotropy that were discussed earlier, through the consideration of lateral/in-plane conductivity.

Previous measurements of the lateral thermal conductivity of Si thin films in SOI structures mainly used electrical resistance thermometry in the steady state (Asheghi et al.,

1997, 1998), where temperature variation at two distinct points (via *in situ* fabricated highly doped areas in the Si films) was measured using an electrical resistance change. Subsequently, the κ was fit using two-dimensional heat conduction models. In another effort (Liu and Asheghi, 2006), measurements on suspended Si thin film membranes, fabricated through wet etching techniques, were performed. However, this methodology requires comparison of a metal heater deposited on a suspended bridge, with and without the Si device layer present, and thermal contact issues related to the sensors could still be significant in the characterization of κ_{ip}. A scanning TR technique was also suggested (Ju and Goodson, 1998) to monitor the transient temperature distribution along the drift region of a SOI power transistor. However, the discrepancy in the trend of values in the earlier data (Asheghi et al., 1997, 1998; Ju and Goodson, 1999) with reduced values in later measurements and theoretical predictions (Liu and Asheghi, 2006) was noted.

We now consider the utility of the TR technique to monitor the κ_{ip} of Si thin films (in the submicron range) in SOI-based structures—Figure 36.2a. The experimental method

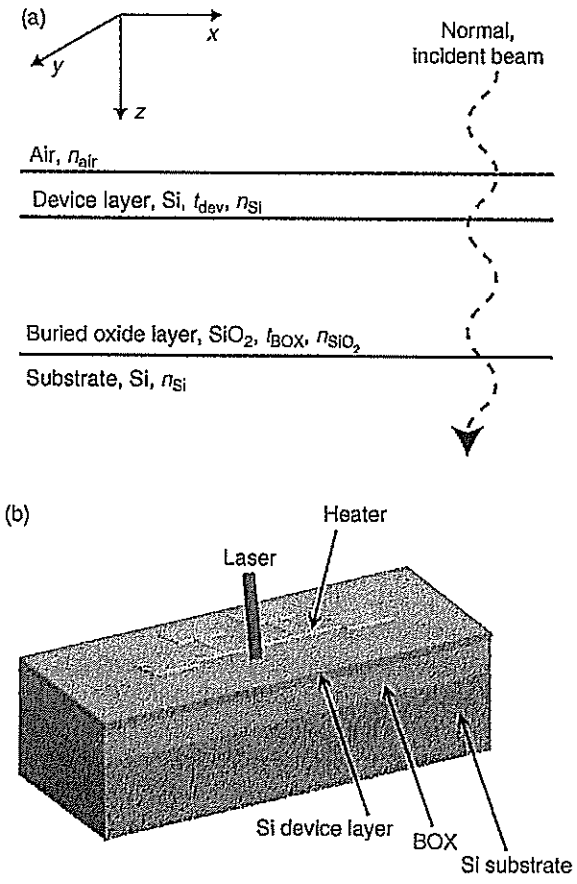

FIGURE 36.2 (a) Schematic of the SOI samples, which provides a test bed for the study of the thermal conductivity of thin Si films. The optical parameters governing the beam–material interactions, n: refractive index, and t: the material thickness, are indicated. (b) A diagram of the experimental principles in the measurement of the temperature profile of a heated SOI sample by rastering a laser beam (e.g., He–Ne laser), as a function of distance from the heater, on the sample surface.

was aimed to avoid thermal contact-related issues through the use of the TR-based temperature sensing. Although the details will be exemplified later the surface temperature gradient in the thin film induced through on-chip heating was monitored—Figure 36.2b. Based on the sensitivity of the TR to sample conditions, it was generally observed that the TR in the visible wavelength range on SOI structures must be carefully calibrated and understood considering the optical transparency and interference effects due to reflections from multiple interfaces, that is, air–Si, Si–SiO_2 (the buried oxide layer, BOX), and SiO_2–Si substrate, all of which are involved in the correlation of the measured TR intensity to the actual sample temperature. The optical response of the sample structure, as manifested through an optical characteristic matrix (OCM) (Born and Wolf, 1964), was then modeled and calculated to predict the device layer thickness at which the TR response is optimal, considering the probe wavelengths (Tessier et al., 2001, 2003) and overlayer thicknesses (Tessier et al., 2001, 2003, 2006; Maize et al., 2008; Ju and Goodson, 1998). A finite-element physics solver was used to calculate the temperature profile in the SOI structure, with the κ_{ip} of the device layer used as the only free parameter to fit the calculated surface temperature to the measured data. Finally, the determined κ_{ip} are compared to theoretical predictions (Chen, 1998; Sondheimer, 1952; Holland, 1963), and the potential application of the method to other film-on-substrate systems are discussed.

36.4 CHARACTERISTICS OF THERMOREFLECTANCE FROM Si THIN FILMS—MODELING AND CALIBRATION

The general principle of the thin film thermal conductivity measurement is that when the surface is heated in a localized region, the temperature distribution in the sample away from the heated region would be a sensitive function of the material properties, such as the κ_{ip}. In addition to surface roughness and contamination effects, any overlayer could also modify the spectral response of the TR, due to internal reflections and interference effects, as mentioned previously. Consequently, it is often preferred, in practice, to predict the C_{TR} using analytical methods, through knowledge of the temperature variation of the refractive index and thermal coefficient of expansion. For example, in the pertinent case of a Si substrate with a silicon dioxide overlayer, the C_{TR} has been derived as a function of thickness of the overlayer (Ju and Goodson, 1998). The reasonable agreement of the calculated values with experimentally measured results suggested that the former can be sufficient for estimation of the overlayer and spectral dependence of the C_{TR}.

The TR contribution of the top Si film/device layer was deconvoluted from the underlying layers/substrate through calculating the sensitivity of the TR intensity to the thickness and temperature of the device layer. The purpose was to show that the TR signal intensity could be maximized through deliberate selection of the device layer thickness through evaluating the reflection matrix of the SOI structure. An interrogation wavelength (λ) corresponding to visible light, that is, at $\lambda = 633$ nm, and geometry, as specified in Figure 36.2 was chosen. The top layer is a single crystalline Si device layer (typically with thickness <250 nm), with an underlying 1-μm SiO_2 (BOX) layer, supported by a 675-μm thick single crystal substrate. From an optical standpoint, the electromagnetic skin depth (Born and Wolf, 1964), d_{Si}, of Si, at $\lambda = 633$ nm, is ~2.3 μm which suggested that incident radiation would penetrate through the Si device layer. The BOX layer was

optically transparent and was modeled with only a real component to the refractive index, while the substrate is much thicker than d_{Si} and is optically opaque.

If the incident radiation modeled as an electromagnetic plane wave and represented through

$$Q_0 = \begin{bmatrix} E_0 \\ H_0 \end{bmatrix}$$

with E_o and H_o as the free-space amplitudes of the electric and magnetic fields, is incident upon a slab of material with refractive index $\tilde{n}_s$, the resultant amplitude at depth z within the slab is given by

$$Q = \begin{bmatrix} E(z) \\ H(z) \end{bmatrix}$$

where $Q_0 = M_s Q$. M_s is the optical characteristic matrix (OCM) of the layered slab, comparing the amplitude of the propagated wave to that of the initial state, and is

$$M_s(z) = \begin{bmatrix} m_s^{11}(z) & m_s^{12}(z) \\ m_s^{21}(z) & m_s^{22}(z) \end{bmatrix} = \begin{bmatrix} \cos\left(\dfrac{2\pi\tilde{n}_s z}{\lambda}\right) & -\dfrac{i}{\tilde{n}_s}\sin\left(\dfrac{2\pi\tilde{n}_s z}{\lambda}\right) \\ -i\tilde{n}_s\sin\left(\dfrac{2\pi\tilde{n}_s z}{\lambda}\right) & \cos\left(\dfrac{2\pi\tilde{n}_s z}{\lambda}\right) \end{bmatrix} \tag{36.6}$$

The electric and magnetic fields are taken to be of the form, $E_x = E(z)e^{i(kz-\omega t)}$ and $H_y = H(z)e^{i(kz-\omega t)}$, respectively. For SOI structures, the M_{SOI}, is equal to the product of the individual OCMs of each optically active layer, that is, the top Si device layer (dev) and the SiO_2 buried oxide (BOX).

$$M_{SOI}(z) = M_{dev}(z)M_{BOX}(z) \tag{36.7}$$

It can then be shown (Born and Wolf, 1964) that the total reflectance of the SOI structure, R_{SOI}, is

$$R_{SOI} = \left|\frac{(m_{SOI}^{11} + m_{SOI}^{12}\tilde{n}_{air})\tilde{n}_{sub} - (m_{SOI}^{21} + m_{SOI}^{22}\tilde{n}_{sub})}{(m_{SOI}^{11} + m_{SOI}^{12}\tilde{n}_{air})\tilde{n}_{sub} + (m_{SOI}^{21} + m_{SOI}^{22}\tilde{n}_{sub})}\right|^2 \tag{36.8}$$

The above equations can be generally used to find the reflectance of any layered structure of arbitrary dimensions, allowing for advanced measurements such as selective probing of nonsurface layers.

A plot of R_{SOI} as a function of the device layer thickness (t_{dev}) at $\lambda = 633$ nm is shown in Figure 36.3a, along with obtained experimental results, and indicated the accuracy of the modeling and experimental calibration. The peaks and troughs in the R_{SOI} are due to interference effects of the incident radiation from boundaries of the device layer. The shape of the variation, that is, broad peaks and narrow troughs, were due to a large refractive index contrast ($\tilde{n}_{dev} - \tilde{n}_{BOX} \sim 2.5$) between the Si device layer and the underlying oxide, and the periodicity was determined by one quarter of the optical path length ($t_{dev}\tilde{n}_{dev}$), where interference interactions will be most influential. It can then be inferred from the $R_{SOI} - t_{dev}$ variation, that the C_{TR} (or dR/dT) could be increased at an optimal

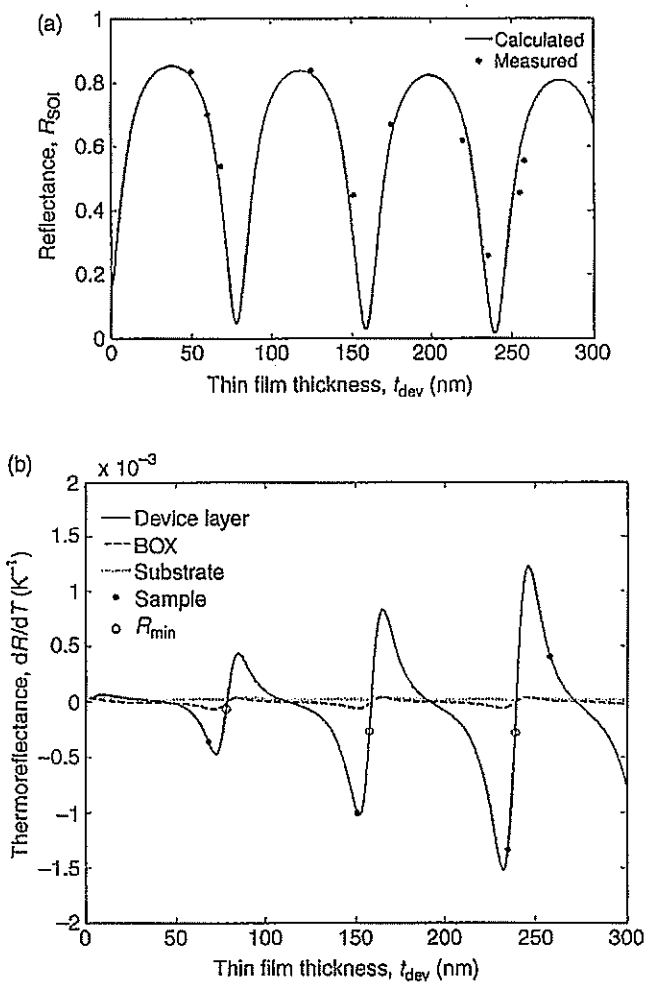

FIGURE 36.3 (a) The calculated and measured optical reflectance (R_{SOI}) of the SOI samples, with varying Si thin film/device layer thickness (t_{dev}). (b) The variation of the temperature derivative of the reflectance (dR/dT) with t_{dev} for the individual layers of the sample, including the top device layer, underlying BOX and the substrate. The values corresponding to the t_{dev} of the measured samples (Sample) and the minima (R_{min})—from Figure 36.3a, are indicated.

t_{dev}. Generally, when any layer of thickness, t, has a temperature variation ΔT, the change of the refractive index and thickness would be $\Delta\tilde{n} = d\tilde{n}/dT\,\Delta T$ and $\Delta t = \xi\Delta T$, respectively, where ξ is the linear thermal coefficient of expansion. For a given SOI sample with a specified device layer thickness, t_{dev}, and an initial temperature, T^0, with reflectance R (T^0, t_{dev}), the change in the net reflectance, ΔR, can be written as:

$$\Delta R = \frac{dR}{dT}\Delta T = R\left(T^0 + \Delta T, t_{dev} + \Delta t,\right) - R\left(T^0, t_{dev}\right) \tag{36.9}$$

For a unit rise in ΔT (= 1 K), and using Equations (36.7) and (36.8), a plot of ΔR versus the t_{dev} was formulated—as in Figure 36.3b, to show the individual $dR_i/dT(i = \text{dev, BOX,}$

or substrate) due to the uniform temperature rise for the ith layer. From an experimental point of view, the observed dR/dT of the SOI structure is modeled as arising from a linear superposition of the individual layers, as follows

$$\frac{dR_{SOI}}{dT} = \frac{dR_{dev}}{dT} + \frac{dR_{BOX}}{dT} + \frac{dR_{han}}{dT} \tag{36.10}$$

Such a model is necessary as the individual contributions of the layers of the SOI are not measurable and was justified on the basis of observations, through computational simulations using MATLAB®, that the difference of dR_{SOI}/dT between (i) that found by considering and summing the individual contributions from each layer (each with a $\Delta T = 1$ K) and (ii) assuming that SOI structure as a whole has $\Delta T = 1$ K, is less than 1%.

The following were then observed from the plot: (1) there is a pronounced modulation of the dR_i/dT which could be either positive/negative, and which is proportional to the slope of R_{SOI}, (2) the dR_{dev}/dT is dominant over that of the other layers by almost two orders of magnitude ($10^{-3}\,K^{-1}$ *vis-a-vis* $10^{-5}\,K^{-1}$) resulting from both the position of the device layer, and the much larger $d\tilde{n}/dT$, and would be the chief contributor to the TR intensity, and that (3) there is a pronounced modulation of the dR_{dev}/dT increasing in amplitude with t_{dev} and exhibiting a maxima whenever there is a minimum in the R (cf., Figure 36.3a), and has the (4) experimental implication that there are select values of t_{dev} where the $dR_{dev}/dT$is maximum/minimum with a corresponding effect on the observed TR intensity. Consequently, the Si thin film thickness (t_{dev}) must be chosen carefully for maximal signal-to-noise ratio in the TR measurements, enabling more accurate determination of the thermal conductivity. Si thin films with $t_{dev} = 68$, 151, 235, and 258 nm were then chosen, corresponding to thicknesses near the maxima of the absolute dR_{dev}/dT shown in Figure 36.3b.

36.5 EXPERIMENTAL PROCEDURES

Si thin films of optimal t_{dev} thickness, following the discussion in Section 36.4, could be fabricated on SOI substrates through reactive ion etching (RIE) of the Si film. A measure of the electrical dopant density should be taken to look at possible effects on the variation of κ (in the work reported here, the density of $\sim 10^{15}/cm^3$ (Taur and Ning, 1998) was not expected to affect the thermal conductivity significantly (Asheghi et al., 2002)). Measurement and calibration of the film thickness was done through spectral reflectance, and error in the measurement was estimated to be less than 5 nm. The surface roughness introduced during the RIE was of the order of a few nanometers. A metal line was then deposited on the Si film surface to serve as an electrical resistance-based heater, for example, see Figure 36.2b. The heater line was constituted of a multilayer of Cr (10 nm)/Au (200 nm) deposited through electron beam evaporation and was typically 10-mm long and 8-μm wide, ensuring a sufficiently high aspect ratio to probe lateral conductivity. To characterize the possible current leakage from the heater into the substrate, 30 nm of SiO_2 was deposited underneath the heater line. However, measurements did not indicate any leakage effects precluding the need for such an oxide. Subsequent to the fabrication of the optimal t_{dev} films, the samples were mounted and wire-bonded to ceramic chip-carriers. Thermal epoxy was used to bond the substrate bottom to the sample holder. The overall sample configuration is schematically shown

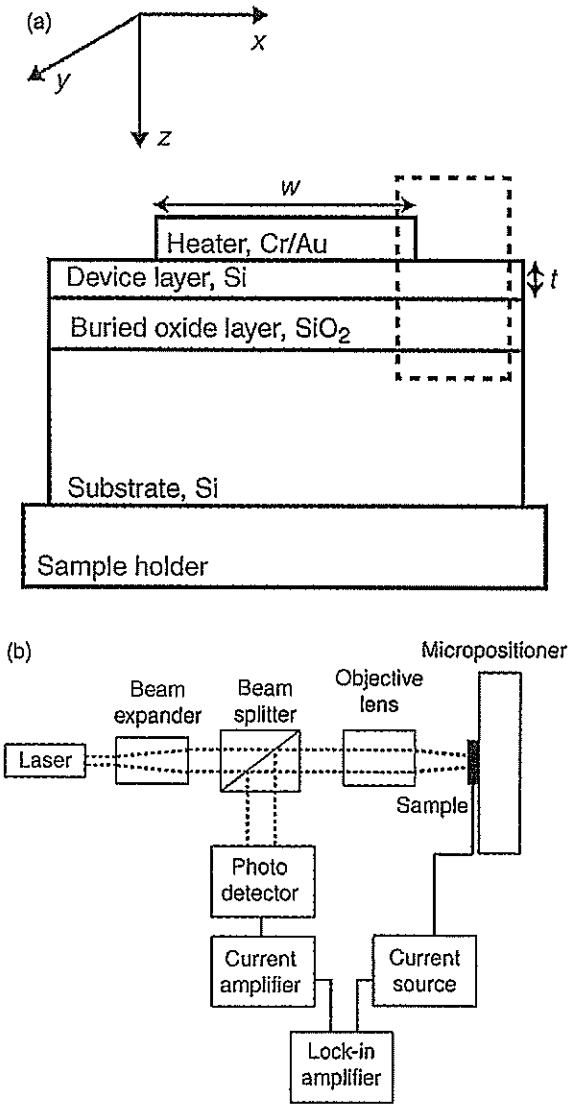

FIGURE 36.4 (a) Schematic of the cross-section of the measured samples (mounted on a chip carrier) with the heater. The lateral heat flow, in the x-direction, in the region delineated by the dotted box, is sensitive to the in-plane thermal conductivity (κ_{ip}) and the corresponding temperature variation along the surface can be estimated. (b) Schematic of the arrangement of apparatus used for the scanning TR thermometry.

in Figure 36.4a, and the setup for the measurement of the TR intensity is indicated in Figure 36.4b. It was assumed that the micropositioner (with $<0.5\ \mu m$ resolution), to which the sample holder was mounted, was an adequate thermal sink and fixed the sample holder bottom to ambient temperature.

A sinusoidal current $I(f)$, at a given frequency f, was passed through the deposited metal line and induced Joule heating (with a harmonic component of $2f$, as derived from

the I^2 component of the heating). AC-based modulation techniques enable accurate lock-in-based detection of the effects of the induced heating with high signal-to-noise ratio. The thermal losses due to convection or radiation can be ignored through the use of time constants (and f values) not overlapping with the characteristic time scales associated with such loss mechanisms. Using lumped thermal analysis (Mills, 1999), it was estimated that, for the device layer thicknesses considered in our experiments, such time scales were of the order of magnitude of 0.01–0.1 s. Consequently, at a heating current frequency, f_h, of ~2.5 kHz, one can safely consider only the conductive heat transfer. Also, the estimated change in the surface temperature due to convective/radiative heat loss was estimated to be less than 1%, through elementary calculations using Newton's law of cooling and the Stefan–Boltzmann Law.

At the chosen f, the thermal wave propagates into the Si substrate, through the top device layer and the BOX. However, due to the orders of magnitude lower κ and much larger thickness of the oxide compared to that of the device layer, it can be assumed that there is a much larger temperature drop across the oxide. Hence, the top device layer is essentially isothermal through the thickness at any given distance from the heater. However, there seems to be significant lateral heat conduction in the BOX near the heater, which modifies the temperature profile of the device layer, and precludes the use of analytic expressions as in earlier studies (Asheghi et al., 1998). Consequently, finite element modeling was necessary to understand such variations, as will be discussed later.

A normally incident, linearly polarized He–Ne laser was then focused onto a heated sample through an objective lens. The spot size could be determined through a knife-edge technique, where the beam was scanned over the metal heater edge onto the Si film surface. Assuming a Gaussian beam profile, with intensity variation given through $I(x) = I_0\exp(-x^2/2r^2)$, the spot radius, r, was found to be as small as ~2 μm. The sample was translated, with 0.2 μm resolution, rastering the focused laser spot across the surface—see Figure 36.2b. The reflected intensity was diverted through a nonpolarized beam splitter onto a diode detector connected to a lock-in amplifier synchronized to $2f$. Both the amplitude (proportional to the temperature fluctuations of the surface) and the phase (related to the sign of the C_{TR}) of the signal were recorded as a function of distance from the heater. The obtained values in the TR measurement were limited by the dark current noise of the detector, which was of the order of 4 nA.

36.6 RESULTS AND DISCUSSION

36.6.1 Determination of the Specific Heat, C, and the Phonon Group Velocity, v_g

A suitable assumed value of the density (ρ) and the specific heat (C) constituting the thermal diffusivity, $\alpha(=\kappa/\rho C)$ of the device layer was necessary before solving/modeling the transient heat conduction equation. Although the density may be assumed to be that of the bulk (CRC Handbook of Chemistry and Physics, 2004), $\rho_{Si} = 2329\,\text{kg/m}^3$, the bulk value of $C \sim 1.67 \times 10^6\,\text{J/m}^3\text{K}$ associated with the "gray" approximation of phonons (Chen, 2005), in which all phonons are treated identically, may not fully characterize their frequency dispersion. A more appropriate value of C which accounts for the phonon dispersion was derived (Chen, 1998; Sondheimer, 1952; Holland, 1963). To illustrate, it was assumed that only the acoustic phonons contribute to heat conduction, while the optical phonons do not, due to their small

group velocity, and that the specific heat capacity associated with heat conduction would be that appropriate for the former group.

The full phonon dispersion in Si, consisting of one longitudinal and two degenerate transverse modes (i.e., LA, TA and LO, TO modes) was considered. Using polynomial fitting functions to analytically describe the experimentally measured acoustic phonon dispersion (Brockhouse, 1959), a $\bar{C}_{\text{avg}} \sim 0.95 \times 10^6\ \text{J/m}^3\text{K}$, was calculated under the Debye model formulation (Kittel, 1996). An average phonon group velocity, $\bar{v}_g$, was also estimated by including the dispersion and normalizing as follows

$$\bar{v}_g = \frac{C_{\text{LA}} v_{g,\text{LA}} + 2C_{\text{TA}} v_{g,\text{TA}}}{\bar{C}_{\text{avg}}} \tag{36.11}$$

The resulting analysis yields $\bar{v}_g = 2274\ \text{m/s}$, which is notably smaller than the value typically considered for bulk, that is, ~6000 m/s. Taking a κ value for Si (~140 W/mK), $\bar{v}_g$, and $\bar{C}_{\text{avg}}$, we obtain an average value of the mean free path, $\bar{l}_{\text{avg}} \sim 200\ \text{nm}$, implying more phonon-boundary interaction in thin films than traditional thermal analysis suggests. Thus, a reduction of κ_{ip} at film thickness near or less than $\bar{l}_{\text{avg}}$ would be expected. Such a framework to understand the reduction of the in-plane thermal conductivity, κ_{ip}, in Si thin films (Narumanchi et al., 2004; Liu and Asheghi, 2006; Mazumder and Majumdar, 2001) and the device layer in SOI substrates (Asheghi et al., 1998; Ju and Goodson, 1999) has been previously established and agrees well with the above calculations.

36.6.2 Finite Element Modeling

As noted earlier, the SOI geometry along with the large aspect ratio of the heater (~40) *vis-à-vis* the device layer thickness (typically, $t_{\text{dev}} < 250\ \text{nm}$) implies a decaying temperature profile from the heater edge—in the x-direction, following Figures 36.2b and 36.4a. Consequently, a two-dimensional analysis of the heat conduction along the cross-section of the sample, perpendicular to the heater axis (i.e., the x–z plane), was pertinent. The Fourier heat conduction equation, for arbitrary geometries, can be solved through a finite element model (FEM) constructed in computational/CAD environments, for example, COMSOL Multiphysics® software, to determine the time-varying temperature along the surface of the device layer in the proximity of the heater and for analyzing the sensitivity of the device layer κ_{ip}. By choosing appropriate free parameters, the calculated temperature profiles could be fit to the measured TR data to elucidate the thermal properties of the device layer.

In accordance with experimental conditions, the following assumptions were used in the model: (1) the heat sink fixes the bottom substrate surface to room temperature, (2) sample surfaces exposed to air were taken to be insulating, that is, $(\text{d}T/\text{d}x)_{\text{surface}} = (\text{d}T/\text{d}z)_{\text{surface}} = 0$, (3) the power per unit area dissipated by the heater at the heater/device layer interface is equal to Joule heat generated by the heating current, and (4) the BOX and Si substrate have bulk thermal properties. The sensitivity of the model solution was examined with respect to the cross-plane thermal conductance, heating power, and frequency. It was found that the surface temperature was unperturbed by variation of the device layer κ_{cp} considered in this work, as well as from the introduction of TBRs at the device layer/BOX and BOX/substrate interfaces, with commonly accepted values (Cahill et al., 2003). The thermal epoxy between the substrate bottom and the

sample holder could introduce a resistance in series with the sink, and was estimated to be $\sim 10^{-3}\,m^2K/W$. However, introduction of the boundary resistance in the model had no effect on the transient component of the surface temperature as the chosen f limits the thermal penetration depth to $\sim 75\,\mu m$ in Si, precluding the interaction of the thermal wave with the bottom of the substrate. In addition, variation of the heating power and frequency within the limits of specified machine error, ~0.1%, did not yield a change in the surface temperature greater than the obtained precision. An example of the calculated temperature profile along the sample cross section near the peak of the heating cycle is shown in Figure 36.5a.

36.6.3 Experimental Measurements of the Lateral Temperature Variation

A typical TR scan, across the surface of the device layer ($t_{dev} = 258\,nm$) indicating the experimental data superposed on calculated temperature profiles with varying κ_{ip} is shown in Figure 36.5b. Each datum represents the maximum amplitude variation of the TR intensity as it varies in time at frequency $2f$, and whose x-coordinate coincides with the center of the probe beam. The error bars due to variation of the TR intensity are also labeled, but are too small to be visible. The magnitude of the TR intensity was scaled such that the values in the limit of $x \to \infty$, for example, when $x \sim 40\,\mu m$ in Figure 36.5b, match the calculated temperature. Although the total TR intensity was an average of the temperature profile convoluted with the spatially distributed intensity of the beam, the resulting measurement was still an accurate indication of the actual temperature at the center of the beam spot (Aubain and Bandaru, 2010). The solid curves represent equivalent, time-variant temperature amplitudes as a function of distance from the heater edge at various modeled κ_{ip}. The goodness-of-fit between the measured results and simulated curves was determined in the range of spatial values where modeled temperature profiles diverged by more than 10%, that is, at $4\,\mu m < x < 30\,\mu m$. The largest correlation coefficient between the scaled TR measurements and calculated temperature values was $R^2 = 0.9999$, corresponding to the fit with $\kappa_{ip} \sim 100\,W/mK$. It was noted that the values of κ_{ip}, matching 60 and 148 W/mK, have R^2 values of 0.9955 and 0.9978, respectively. While correlation remains high for the given calculated temperature profiles, their relative values could be used to indicate the most appropriate κ_{ip} so as to closely match experimental data.

Figure 36.5c shows the measured TR signal phase of the heat wave peak as a function of the distance from the heater, where decreasing phase indicates greater lag with respect to the heating frequency reference. The phase was a direct indication of the difference in sign of dR_{dev}/dT between samples of different thickness (cf., Figure 36.3). More specifically, comparing the signs of the dR_{dev}/dT for $t_{dev} = 258\,nm$ to other device thicknesses, that is, $t_{dev} = 68$, 151, and 235 nm, the former has a positive value while the latter have negative values. Consequently, the lock-in measurement of two TR signals with identical phase but opposite sign would be manifested in a π phase shift, as indicated in Figure 36.5c. It was also noted that the TR signal phase did not indicate a π phase shift as the beam was rastered from the Au heater line to the device layer, implying that $dR_{dev}/dT$and dR_{Au}/dT are of the same sign. As it was previously established that dR_{Au}/dT is negative at $\lambda = 633\,nm$ (Tessier et al., 2001; Raad et al., 2008; Christofferson et al., 2001), the dR_{dev}/dT of these SOI samples at these thickness must be negative as well, further supporting the OCM predictions plotted in Figure 36.3.

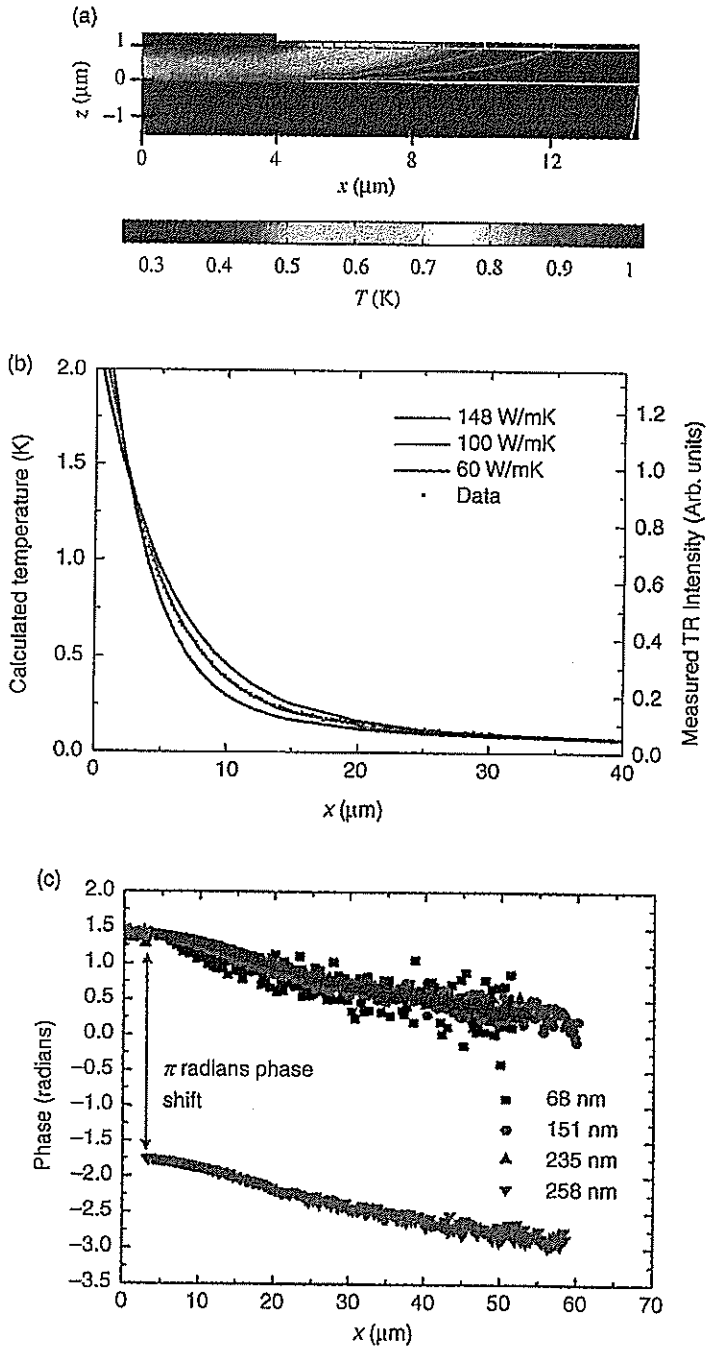

FIGURE 36.5 (a) Modeled variation, through FEM, of the temperature along the sample cross-section, indicated at the peak of a given heating cycle. (b) A typical TR scan across the surface of the device layer ($t_{dev} \sim 250$ nm) indicating the experimental data superposed on modeled temperature profiles with varying κ_{ip}. The error bars are too small to be visible. (c) The measured TR signal phase of the heat wave peak as a function of the distance from the heater is a direct indication of the difference in sign of TR intensity between samples of different thickness, cf., Figure 36.3b.

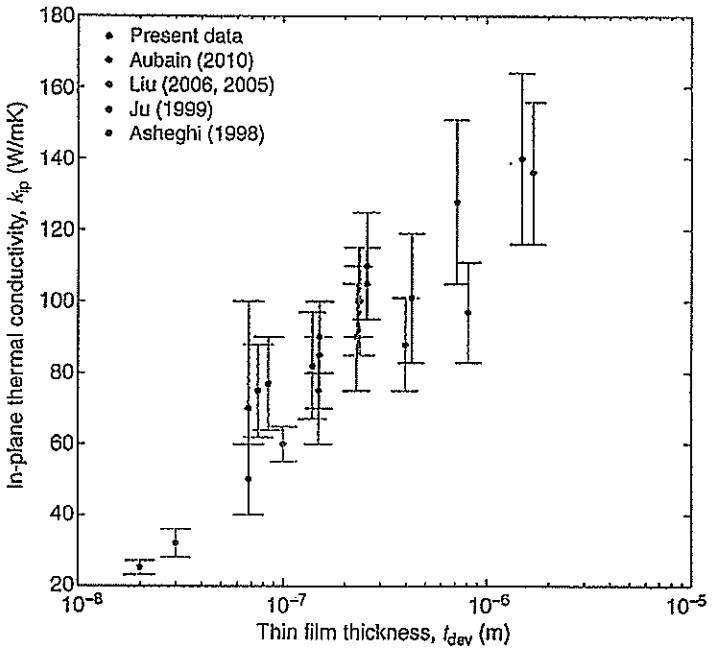

FIGURE 36.6 A comparison of the thermal conductivity values (obtained from the TR intensity fits in the present work) with those obtained previous literature (Aubain et al. 2010; Liu et al. 2005, 2006; Ju et al. 1999; Asheghi et al. 1998).

36.6.4 Estimation of the In-plane Thermal Conductivity of Si Thin Films

The principles outlined above were used to determine the values of the κ_{ip} and compare with the results obtained by other previous measurements (Ju and Goodson, 1999; Aubain and Bandaru, 2010), which have been plotted in Figure 36.6. Generally, a decreasing κ_{ip} is observed with respect to t_{dev}. The high accuracy and precision of the data obtained in this work—as in Figure 36.5b, stems from the accuracy in modeling as well as improved spatial resolution. Most notably, there seems to very good agreement between our measured κ_{ip} and those obtained through measurements with suspended Si structures fabricated from SOI substrates (Liu and Asheghi, 2006). Generally, suspended beam geometry greatly simplifies thermal analysis due to the restriction on heat conduction paths. However, fabrication of such geometries is elaborate and nontrivial involving controlled wet etching and is often not easily implemented for many thin films of interest, for example, those lacking a sacrificial intermediate layer. The comparison of the κ_{ip} previously measured through electrically resistive elements of suspended (Liu and Asheghi, 2006) and supported (Asheghi et al., 1997, 1998; Ju and Goodson, 1999) Si films show that measurements of supported samples seem to be less sensitive to the film properties (Ju and Goodson, 1999) or have high variability (Asheghi et al., 1998).

36.7 SUMMARY AND OUTLOOK

The modulation of reflected light as a function of the surface temperature of the material forms the basis of TR, and has been discussed in this work as a means to understand the

thermal conductivity (κ) of lower dimensional structures such as submicron thickness thin films. The TR response (both the magnitude and the sign) was found to be sensitive to the thickness of the thin film layer and modeled using an optical characteristic matrix formulation to choose appropriate thin film thicknesses. High aspect ratio, on-chip heating elements produced temperature profiles that were measured as a function of distance with respect to the heater edge, and the profiles were fit to a robust finite element model with the in-plane thermal conductivity (κ_{ip}) as the only free parameter. Comparison of the obtained thermal conductivity values with previous measurements confirms the validity of the technique and suggests that complete isolation of the thin film, as in earlier methodologies, from the substrate may not be required.

The advantage of the use of such optical methods to determine the κ is the possible elimination of electrical resistance-based sensing/thermometry, which suffers from thermal boundary resistance-related issues, which vary from device to device due to contact-material interfaces. The proposed TR-based methodology then provides a quick, noncontact-based optical metrology to determine the temperature profiles and thermal energy distributions.

In probing the frontiers of scientific and technological research, it is of interest to explore experimental techniques for the determination of the κ tensor, which could then yield insight, for example, into the relevance of the isotropy assumption prevalent in the literature. It would be reasonable to expect that anisotropy influences would be manifest in lower symmetry crystal structures as well as lower dimensional materials, such as two-dimensional thin films or one-dimensionally oriented nanowires and the methods described here may be useful in such investigations.

ACKNOWLEDGMENTS

We gratefully acknowledge support from the National Science Foundation (Grant ECS 0643761). The assistance of B. Fruhberger and R. Anderson at the Nano3 facility at UC, San Diego and discussions with A. Arriagada, M. Gollner, and R. Mifflin are appreciated.

REFERENCES

Arriagada A, Yu ET, Bandaru PR. Determination of thermal parameters of one-dimensional nanostructures through a thermal transient method. *Journal of Thermal Analysis* 2009;97:1023–1026.

Asheghi M, Kurabayashi K, Kasnavi R, Goodson KE. Thermal conduction in doped single-crystal silicon films. *Journal of Applied Physics* 2002;91:5070–5088.

Asheghi M, Leung YK, Wong SS, Goodson KE. Phonon-boundary scattering in thin silicon layers. *Applied Physics Letters* 1997;71:1798–1800.

Asheghi M, Touzelbaev MN, Goodson KE, Leung YK, Wong SS. Temperature-dependent thermal conductivity of single-crystal silicon layers in SOI substrates. *Journal of Heat Transfer* 1998;120:30–36.

Aubain M, Bandaru PR. Determination of diminished thermal conductivity in silicon thin films using scanning thermoreflectance thermometry. *Applied Physics Letters* 2010;97:253102.

Baba T, Ono A. Improvement of the laser flash method to reduce uncertainty in thermal diffusivity measurements. *Measurement Science & Technology* 2001;12:2046–2057.

Baillis D, Randrianalisoa J. Prediction of thermal conductivity of nanostructures: Influence of phonon dispersion approximation. *International Journal of Heat and Mass Transfer* 2009;52:2516–2527.

Bandaru PR. Electrical properties and applications of carbon nanotube structures. *Journal of Nanoscience and Nanotechnology* 2007;7:1239–1267.

Berglund CN. Temperature-modulated optical absorption in semiconductors. *Journal of Applied Physics* 1966;37:3019.

Borca-Tasciuc T, Kumar AR, Chen G. Data reduction in 3w method for thin-film thermal conductivity determination. *Review of Scientific Instruments* 2001;72:2139–2147.

Born M, Wolf E. *Principles of Optics*. New York: Pergamon Press; 1964.

Boukai AI, Bunimovich Y, Tahir-Kheli J, Yu J-K, Goddard III, WA, Heath JR. Silicon nanowires as efficient thermoelectric materials. *Nature* 2008;451:168–171.

Brockhouse BN. Lattice vibrations in silicon and germanium. *Physical Review Letters* 1959;2:256–258.

Cahill DG. Thermal conductivity measurement from 30 to 750 K: the 3w method. *Review of Scientific Instruments* 1990;61:802–808.

Cahill DG, Goodson KE, Majumdar A. Thermometery and thermal transport in micro/nanoscale solid-state devices and structures. *Journal of Heat Transfer* 2002;124:223–241.

Cahill DG, Ford WK, Goodson KE, Mahan GD, Majumdar A, Maris HJ, Merlin R, Phillpot SR. Nanoscale thermal transport. *Journal of Applied Physics* 2003;93:793–818.

Capinski WS, Maris HJ. Improved apparatus for picosecond pump-and-probe optical measurements. *Review of Scientific Instruments* 1996;67:2720–2726.

Capinski WS, Maris HJ, Ruf T, Cardona M, Ploog K, Katzer DS. Thermal-conductivity measurements of GaAs/AlAs superlattices using a picosecond optical pump-and-probe technique. *Physical Review B* 1999;59:8105–8113.

Carslaw HS, Jaeger JC. *Conduction of Heat in Solids*. 2nd ed. New York: Oxford University Press; 1986.

Che J, Cagin T, Goodard WA. Thermal conductivity of carbon nanotubes. *Nanotechnology* 2000;11:65–69.

Chen G. Thermal conductivity and ballistic phonon transport in the cross-plane direction of superlattices. *Physical Review B* 1998;57:14958–14973.

Chen G. *Nanoscale Energy Transport and Conversion*. New York (NY): Oxford University Press; 2005.

Chen G. Particularities of heat condcution in nanostructures. *Journal of Nanoparticle Research* 2000;2:199–204.

Chen G, Shakouri A. Heat transfer in nanostructures for solid-state energy conversion. *Transactions of the ASME* 2002;124:242–252.

Chen Y, Li D, Yang J, Wu Y, Lukes JR, Majumdar A. Molecular dynamics study of the lattice thermal conductivity of Kr/Ar superlattice nanowires. *Physica B: Condensed Matter (Amsterdam)* 2004;349:270–280.

Christofferson J, Maize K, Ezzahri Y, Shabani J, Wang X, Shakouri A. Microscale and nanoscale thermal characterization methods. *Journal of Electronic Packaging* 2008;130:041101.

Christofferson J, Vashaee D, Shakouri A, Melese P. Real time sub-micron thermal imaging using thermoreflectance. International Mechanical Engineering Congress and Exhibition New York (NY); 2001.

CRC Handbook of Chemistry and Physics. 85th edition, D. Lide [Ed.], CRC Press; 2004.

Dolling G, Cowley RA. The thermodynamic and optical properties of germanium, silicon, diamond and gallium arsenide. *Proceedings of the Physical Society* 1966;88:463–494.

Fox M. *Optical Properties of Solids*. New York (NY): Oxford University Press; 2001.

Holland MG. Analysis of lattice thermal conductivity. *Physical Review* 1963;132:2461–2471.

Ju YS, Goodson KE. Short-time-scale thermal mapping of microdevices using a scanning thermoreflectance technique. *Journal of Heat Transfer* 1998;120:306–313.

Ju YS, Goodson KE. Phonon scattering in silicon films with thickness of order 100 nm. *Applied Physics Letters* 1999;74:3005–3007.

Kelly MJ. Acoustic phonon transmission in superlattices. *Journal of Physics C: Solid State Physics* 1985;18:5965–5973.

Kittel C. *Introduction to Solid State Physics*. New York: John Wiley; 1996.

Koh YK, Cao Y, Cahill DG, Jena D. Heta-transport mechanisms in superlattices. *Advanced Functional Materials* 2009;19:610–615.

Lee S-M, Cahill DG. Heat transport in thin dielectric films. *Journal of Applied Physics* 1997;81:2590–2595.

Lee SM, Cahill DG. Thermal conductivity of Si-Ge superlattices. *Applied Physics Letters* 1997;70:2957–2959.

Little WA. The transport of heat between dissimilar solids at low temperatures. *Canadian Journal of Physics* 1959;37:334–349.

Liu W, Asheghi M. Thermal conductivity measurements of ultra-thin single crystal silicon layers. *Journal of Heat Transfer* 2006;128:75–83.

Maize K, Ezzahri Y, Wang X, Singer S, Majumdar A, Shakouri A. Measurement of thin film isotropic and anisotropic thermal conductivit using 3-omega and thermoreflectance imaging. 24th IEEE Semi-Therm Symposium 2008:185.

Mayer PM, Luerßen D, Ram RJ, Hudgings J. Theoretical and experimental investigation of the resolution and dynamic range of CCD-based thermoreflectance imaging. *Journal of the Optical Society of America A: Optics and Image Science* 2006;25:1156–1163.

Mazumder S, Majumdar A. Monte carlo study of phonon transport in solid thin films including dispersion and polarization. *Journal of Heat Transfer* 2001;123:749–759.

Mills AF. *Basic Heat & Mass Transfer*. 2nd ed. Upper Saddle River: Prentice Hall; 1999.

Narumanchi SVJ, Murthy JY, Amon CH. Submicron heat transport model in silicon accounting for phonon dispersion and polarization. *Journal of Heat Transfer* 2004;126:946–955.

Narumanchi SVJ, Murthy JY, Amon CH. Comaprison of different phonon transport models for predicting heat conduction in silicon-on-insulator transistors. *Journal of Heat Transfer* 2005;127:713–723.

Ohring M. *Materials Science of Thin Films*. 2nd ed. San Diego: Academic Press, 2002.

Ozisik N. *Boundary Value Problems of Heat Conduction*. New York(NY): Dover Publications Inc.; 1968.

Paddock CA, Eesley GL. Transient thermoreflectance from thin metal films. *Journal of Applied Physics* 1986;60:285–290.

Parker WJ, Jenkins RJ, Butler CP, Abbott GL. Flash method of determining thermal diffusivity, heat capacity, and thermal conductivity. *Journal of Applied Physics* 1961; 32:1679–1684.

Peierls RE. *Quantum Theory of Solids*. Oxford (UK): Oxford University Press; 1955.

Pollack GL. Kapitza resistance. *Reviews of Modern Physics* 1969;41:48–81.

Pop E. Energy dissipation and transport in nanoscale devices. *Nano Research* 2010;3:147–169.

Quelin X, Perrin B, Peretti P. Three-dimensional thermal-conductivity-tensor measurement of a polymer crystal by photothermal probe-beam deflection. *Physical Review B* 1993;48:3677–3682.

Raad PE, Komaraov PL, Burzo MG. Thermal characterization of embedded electronic features by an integrated system of CCD thermography and self-adaptive numerical modeling. *Microelectronics Journal* 2008;39:1008–1015.

Rosencwaig A, Opsal J, Smith WL, Willenborg DL. Detection of thermal waves through optical reflectance. *Applied Physics Letters* 1985;46:1013–1015.

Saleh BEA, Teich MC. *Fundamentals of Photonics*. 2nd ed. Hoboken, NJ: John Wiley & Sons; 2007.

Schmidt AJ, Chen X, Chen G. Pulse accumulation, radial heat conduction, and anisotropic thermal conductivity in pump-probe transient thermoreflectance. *Review of Scientific Instruments* 2008;79: 114902-1-9.

Schmidt AJ, Cheaito R, Chiesa M. A frequency-domain thermoreflectance method for the characterization of thermal properties. *Review of Scientific Instruments* 2009;80: 094901-1-6.

Sondheimer EH. The mean free path of electrons in metals. *Advances in Physics* 1952;1:1–42.

Stoner RJ, Maris HJ. Kapitza conductance and heat flow between solids at temperatures from 50 to 300K. *Physical Review B: Condensed Matter* 1993;48:16373–16387.

Swartz ET, Pohl RO. Thermal boundary resistance. *Reviews of Modern Physics* 1989;61:605–668.

Sze SM. *Semiconductor Devices: Physics and Technology*. 2nd ed. Singapore: John Wiley & Sons, Inc.; 2003.

Sze SM, Ng KK. *Physics of Semiconductor Devices*. Hoboken, New Jersey: Wiley-Interscience; 2006.

Taur Y, Ning TH. *Fundamentals of Modern VLSI Devices*. New York: Cambridge University Press; 1998.

Tessier G, Holé S, Fournier D. Quantitative thermal imaging by synchronous thermoreflectance with optimized illumination wavelengths. *Applied Physics Letters* 2001;78:2267–2268.

Tessier G, Jerosolimski G, Holé S, Fournier D, Filloy C. Measuring and predicting the thermoreflectance sensitivity as a function of wavelength on encapsulated materials. *Review of Scientific Instruments* 2003;74:495.

Tessier G, Jerosolimski G, Holé S, Fournier D, Filloy C. Measuring and predicting the thermoreflectance sensitivity as a function of wavelength on encapsulated materials. *Review of Scientific Instruments* 2003;74:495–499.

Tessier G, Polignano M-L, Pavageau S, Filloy C, Fournier D, Cerutti F, Mica I. Termoreflectance temperature imaging of integrated circuits: calibration technique and quantitative comparison with integrated sensors and simulations. *Journal of Physics D: Applied Physics* 2006;39:4159–4166.

Volz S, Chen G. Molecular dynamics simulation of thermal conductivity of silicon nanowires. *Applied Physics Letters* 1999;75:2056–2058.

37

SELECTION OF METALS FOR STRUCTURAL DESIGN

MATTHEW J. DONACHIE

Handbook of Measurement in Science and Engineering, 2V Set, First Edition. Edited by Myer Kutz.